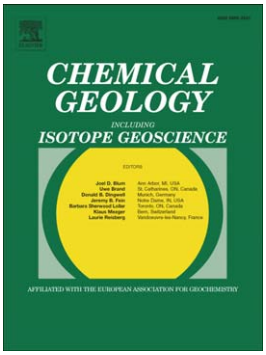

Oxygen isotope fractionation between calcite and fluid as a function of growth rate and temperature: An *in situ* study

R.I. Gabitov, E.B. Watson

PII: S0009-2541(12)00113-1
DOI: doi: 10.1016/j.chemgeo.2012.02.021
Reference: CHEMGE 16462

To appear in: *Chemical Geology*

Received date: 1 November 2011
Revised date: 17 February 2012
Accepted date: 24 February 2012

Please cite this article as: Gabitov, R.I., Watson, E.B., Oxygen isotope fractionation between calcite and fluid as a function of growth rate and temperature: An *in situ* study, *Chemical Geology* (2012), doi: 10.1016/j.chemgeo.2012.02.021

Oxygen isotope fractionation between calcite and fluid as a function of growth rate and temperature: An *in situ* study.

Gabitov R.I.[1] and Watson E.B.[2]

[1] University of California, Los Angeles, CA, USA

[2] Rensselaer Polytechnic Institute, Troy, NY, USA

Abstract

The ^{18}O content of carbonates (expressed as $\delta^{18}O$) is widely used in paleothermometry, yet it is clear from comparison of experimental results and natural carbonate samples that chemical (isotopic) equilibrium is not always achieved in nature. This observation underscores the importance of exploring possible effects of growth rate on isotopic fractionation, which is the focus of this study. *In situ* Secondary Ion Mass Spectrometry (SIMS) analyses of $\delta^{18}O$ were performed on single crystals of experimentally grown calcite. The change in growth rate (V) over time within each crystal was monitored by addition of multiple rare earth element (REE) spikes into the fluid from which the calcite grew. The values of $\delta^{18}O$ in bulk calcites and experimental fluids were measured by stable isotope ratio mass spectrometers. The average SIMS $\delta^{18}O$ overlaps with those determined by conventional mass spectrometry within analytical uncertainty. The fractionation factor expressed as $\Delta^{18}O$ approaches its equilibrium value in slowly grown calcites (V<0.02 nm/s) and decreases by 1.5 ‰ with increasing growth rate from 10^{-3} to 0.34 nm/s. Here $\Delta^{18}O=10^3 \cdot \ln(\alpha^{18}O)$, and $\alpha^{18}O = (^{18}O/^{16}O)_{calcite}/(^{18}O/^{16}O)_{fluid}$. Our results provide the first *in situ* evidence that under equilibrium conditions ^{18}O may be depleted in the near-surface region of calcite relative to the bulk crystal lattice, and that this ^{18}O-depleted zone can be "captured" during rapid crystal growth. Crystal growth rate is therefore a potentially important consideration when using $\delta^{18}O$ in natural carbonates as a proxy for ocean and terrestrial temperature.

Keywords:
Calcite
Oxygen isotopes
Isotopic fractionation factor
Growth rate
SIMS
Temperature
Equilibrium

Introduction

The oxygen isotope compositions of marine and continental carbonates and speleothems are widely used in paleoclimatology (Epstein et al. 1953; Broecker 1986; Labeyrie et al. 1987; Lea et al. 2000; etc.). However, there are certain complications in $\delta^{18}O$-based temperature reconstruction. Among them is the presence of isotopic heterogeneity in biogenic and abiogenic calcites grown at constant environmental conditions (Owen et al. 2002; Rollion-Bard et al. 2008; Dietzel at al. 2009; Barras et al. 2010; etc.). In addition, the $\delta^{18}O$ value of the natural fluid growth media of biogenic and inorganic calcium carbonate is generally unknown. *In situ* SIMS analyses have shown that $\delta^{18}O$ varies between two different zones of individual foraminiferal shells (Rollion-Bard et al. 2008). These authors discovered that early precipitated (primary) calcite is depleted in $\delta^{18}O$ by 3 ‰ relative to later precipitated (secondary) calcite, even though both calcite types are biominerals belonging to the foraminifera and are not the result of alteration. The $\delta^{18}O$ depletion of the primary calcite was explained by elevated pH at the onset of precipitation, which causes an increase of isotopically light CO_3^{2-} component in the calcifying fluid (Usdowski and Hoefs 1993; Erez 2003; Grinstein et al. 2004; Bentov and Erez 2006; Zeebe 1999 and 2007). Experimental studies of inorganically precipitated calcite have revealed that the growth rate, V, affects the uptake of trace and minor elements into the crystal lattice (Lorens 1981, Tesoriero and Pankow 1996, Gabitov and Watson 2006, Tang et

al. 2008a). The factor(s) responsible for this disequilibrium effect might also apply to stable isotope incorporation during calcite growth (Watson 2004; Gabitov and Watson 2005, Tang et al. 2008b; Dietzel et al. 2009).

In our work we use SIMS to evaluate, *in situ*, the effect of V on $\alpha^{18}O_{calcite\text{-}H_2O}$ ($\alpha^{18}O_{calcite\text{-}H_2O}$ will be referred to as $\alpha^{18}O$ hereafter). The advantage of SIMS over conventional bulk mass spectrometry is the ability to obtain data from regions as small as a few microns in size. This high spatial resolution makes it possible to examine variations in isotope ratios within individual crystals, and to quantify the effect of the actual crystal growth rate—as opposed the (bulk) mass precipitation rate—on isotopic composition. Other *in situ* techniques (i.e., electron probe and laser-ablation ICP-MS) can achieve similar spatial resolution, but they are not capable of measuring oxygen isotopic composition. The improvement in analytical spatial resolution to micron scales leads to higher temporal resolution of past changes through studying of carbonate archives. Here for the first time we show that plausible variations in V can affect $\alpha^{18}O$ in a single crystal of calcite grown at constant temperature. The intra-crystalline values of $\alpha^{18}O$ vary by 1-3 ‰, potentially causing an offset in the temperature estimate by 5-15°C.

In this study we monitor the growth rate of calcite crystals by injecting rare-earth element (REE) spikes into the growth medium at discrete intervals during growth. Because the REE are taken up into the growing calcite, this procedure yielded four to eight "marker horizons" within individual crystals, between which the growth rate could be calculated (Figure 1). The value of $\alpha^{18}O$ decreases with increasing V (i.e., high V causes disequilibrium in $\alpha^{18}O$), which is consistent with growth entrapment of an isotopically distinct near-surface region of the calcite crystals: if V exceeds a critical value above which equilibrium is no longer maintained

by local diffusion, then the crystal surface may be "captured" by the newly-formed lattice (Watson 2004). The direction of our trend is consistent with those of Dietzel et al. (2009) and Day and Henderson (2011). In contrast to our direct estimation of crystal growth rate, however, these authors characterized precipitation rate in terms of μmol/(m^2h) or calcite-bearing fluid drips per minute, and bulk $\delta^{18}O$ analyses were conducted on a mass of calcite crystals. For this reason, neither inter- nor intra-crystal variability in $\delta^{18}O$ could be assessed in these studies. A key additional aspect of our study is that the ranges in growth rate and temperature of our synthetic calcites overlap with those of natural (biogenic) $CaCO_3$, making our work potentially relevant to natural materials (ter Kuile and Erez, 1984; Baker et al., 1998; Stoll et al., 2002; Owen et al., 2002; Freitas et al., 2008).

Experimental and analytical methods

Calcite precipitation

Our calcite growth method was adapted from the approach of Gruzensky (1967) and modified by introduction of sub-sampling and multiple REE spikes. The initial solution was prepared by dissolving NH_4Cl in deionized (DI) H_2O to the concentration of 0.5 mol/l, along with minor amounts of reagent grade $CaCl_2{\cdot}2H_2O$ (0.01), $MgCl_2{\cdot}6H_2O$ (10^{-3}), $SrCl_2{\cdot}6H_2O$ (10^{-4}), $BaCl_2{\cdot}2H_2O$ ($2{\cdot}10^{-5}$), $LiOH{\cdot}H_2O$ ($5{\cdot}10^{-4}$), H_3BO_3 (0.01), and U ICP-MS standard (10^{-5}) [values in parentheses are concentrations in mol/l]. The pH of the solution was adjusted to 5.5 by addition of reagent grade NaOH. This initial solution was used as the starting growth medium in all experiments. In order to achieve faster nucleation, the starting growth medium was pre-saturated in CO_2 by full exposure to a CO_2- and NH_3-bearing atmosphere created by decomposition of ammonium carbonate, until the pH exceeded 7.5. No crystals were observed after this prodecure; the resulting state will be refered as "initial saturation" later in the text.

The subsequent CO_2 flux from the atmosphere to the fluid growth medium was reduced by partially closing the container lids, and the containers were placed in environments maintained at different temperatures. Pyramid-shaped calcite crystals grew outward from the bottom and the walls of the containers held at temperatures of 15±0.10°C (DC-15), 19.7±0.25°C, 21.7±0.10°C (DC-3), and 24.6±0.10°C (DC-1). Relatively long runs (DC-15 and DC-1) were conducted in a T -controlled bath. Shorter experiments (DC-3 and DSC-4) were conducted at room temperature, which was routinely monitored *in situ* by thermocouple with a precision of ±0.10°C, which is smaller than the actual temperature variation in the room. In order to encourage growth of crystals large enough for SIMS analyses, the fluids were not stirred during calcite precipitation. However, the solutions were mixed after addition of each REE spike by repeated injection and withdrawal of fluid using a 60-ml syringe. REE spikes (Sm, La, Nd, Tb, and Pr) were sequentially introduced into the growth medium in the amount of 1 ml of diluted REE-bearing solution, which yielded an estimated REE concentration range in the solution from 0.1 to 0.5 ppb. Rare-earth elements are highly compatible in calcite (Zhong and Mucci 1995), so their injection into the growth solutions provided convenient time markers in the crystals. The first REE spike (Sm) was introduced into solution as soon as the calcite crystals became visible with the naked eye. The onset of nucleation was not determined directly, but was estimated from the time interval between two visual observations. The fluids were sampled periodically for measurement of pH, and stored in a refrigerator for future use. The pH (NBS-scale) was measured immediately after collection of the fluid using an OAKTON pH 510 meter with "All-in-One" pH/Temp electrode calibrated with 7.00 and 10.00 pH buffers stored at the same temperature as the experiments. As noted previously, the pH of the initial fluid was 5.5. Subsequent pH measurements collected after initial saturaton of the

fluid are presented in Figure S-1. In run DC-1 (24.6°C), the pH increased slowly during calcite precipitation from about 7.96±0.06 to 8.17±0.02 (Table 1). In the other experiments (DC-15, DC-3, and DSC-4), the pH during the main interval of calcite growth was not measured directly because precipitation began before addition of Sm. At the time of Sm addition, the pH in DC-3, and DSC-4 and DC-15 was 7.83, 7.85, and 8.37, respectively (Figure S-1). At the end of the runs, calcite crystals were recovered with a stainless steel or plastic spatula and quickly rinsed with DI H_2O and methanol.

Bulk analyses of calcite and fluids

Calcite crystals and fluids were analyzed for $\delta^{18}O$ in the Stable Isotope Laboratory at the University of California, Davis. Bulk analyses of calcite crystals were performed with a Fisons Optima IRMS using a common acid bath at 90°C. Fluid samples were analyzed with a Finnigan MAT 251 IRMS with an online CO_2 equilibration system. The mass spectrometer measures the $\delta^{18}O$ between standard and reference value 10 times. The internal precision is 1 standard error (1 s.e.=0.05 ‰) of the measurement of the same gas over a 5 minute period. Calcites were dissolved within one aliquot; fluids were loaded into several vials.

Calcium analyses of the fluids were performed using ICP-OES (*Varian VISTA PRO*™) at the School of GeoSciences, University of Edinburgh. Dissolved inorganic carbon (DIC) was determined using the coulometric SOMMA (Single-Operator Multi-Metabolic Analyzer) system in the Biogeochemistry Laboratory at UCLA (for details see Johnson et al., 1993).

In situ analyses of calcites

Sample preparation

The largest calcite crystals were mounted in epoxy (EpoxiCure®, Buehler) such that the pyramid base (the crystal side adjacent to the substrate during growth) was exposed for SIMS

analysis. The mounts were polished and the crystals were examined with CAMECA ims 1270 ion microprobe at UCLA, first for Ca and REE and subsequently for oxygen isotopes.

Ca and REE analyses by SIMS

Calcium and REE were measured with a 3-18 nA $^{16}O^-$ primary beam at 20-30μm lateral dimension on the sample surface. Positive secondary ions corresponding to mass/charge stations of 41.7 (background), ^{42}Ca, ^{139}La, ^{141}Pr, ^{143}Nd, ^{149}Sm, and ^{159}Tb were measured in mono collection mode with electronic multiplier. To reduce molecular interferences, Ca and REE were analyzed with a sample voltage offset of -60 V using the energy bandwidth of 50 V (total voltage was 10 kV). Intensities were measured by peak switching with waiting times of 1-3 s and counting times of 1 and 10 s for ^{42}Ca and REE, respectively. Previous studies have established that the analytical method described above is sufficient to reduce potential molecular interferences for ^{42}Ca to < 0.1% (Hart and Cohen, 1996). Rare-earth analyses revealed regions of the crystals representative of specific calcite growth intervals, and thus allowed reconstruction of the evolution of growth over time. Following REE determinations, the mount was polished to remove about 2 μm of calcite and analyzed for $\delta^{18}O$ at the same x-y coordinates used for REE measurements. Because of the re-polishing, a small shift in x-y coordinates of the metal and oxygen isotope analyses is possible, but this is insignificant relative to the size of the ion beam (20-30 μm; see below).

$\delta^{18}O$ analyses by SIMS

Individual crystals were examined with a 2-3 nA Cs^+ primary beam with a lateral dimension of 20-30 μm at the sample surface. Negative secondary ions ^{16}O and ^{18}O were simultaneously measured by Faraday Cups (FC) using multicollection set-up for a mass resolving power (MRP) of ~2000, which is sufficient for resolving hydride interference with the ^{18}O peak

(Fayek et al. 2002). During two analytical sessions the raw intensity of the minor isotope varied from $4{\cdot}10^6$ to $5{\cdot}10^6$ counts per second (cps). Raw intensities were corrected for FC background that was measured during the analysis period for each detector. Each spot analysis started with 30 s pre-sputtering followed by automatic field aperture and entrance slit centering for 90 s. The total sputtering time prior to acquisition was therefore 120 s, which was sufficient to reach a steady $^{18}O/^{16}O$ value over the 12 cycles of the analysis on a single spot. In order to quantify SIMS data, sample raw $^{18}O/^{16}O$ ratios were normalized to those of NBS-19 (located in the same mount), where $^{18}O/^{16}O = 0.0020626$ and $\delta^{18}O(PDB) = -2.20$ (Friedman et al. 1982). No mass fractionation between calcite standards (NBS-18 carbonatite, NBS-19 limestone) and experimental calcite was observed; i.e., the average $^{18}O/^{16}O$ of DC-1 calcite lay on the standards calibration line within uncertainty (1s.d.=0.5 ‰). NBS-19 was analyzed routinely after every 5-8 measurements of the experimental calcites, and both NBS-18 and NBS-19 yielded typical reproducibility of 0.3‰ (n=10).

The synthetic calcite crystals were characterized with SIMS spot profiles (traverses) from the crystal center to edge. Imaging with an interference microscope (PHASE SHIFT MicroXAM Surface Mapping Microscope Crystal) revealed slight relief on the sample surfaces in the sense that the calcite edges were elevated 0.6-0.9 μm above the crystal centers. Similar relief of <1 μm was noted on the carbonate standard grains (NBS-18 and NBS-19). All crystals examined were located at the within ~7 mm of the center of the 25.4-mm dia. epoxy mount containing them. According to Kita et al. (2009) the relief and sample positioning described above should not affect $\delta^{18}O$ measurements in silicate minerals. In addition, two 10 mm long profiles with 1 mm steps in X and Y directions (X,Y=0 in the center of the mount) on the glass slide confirmed that $\delta^{18}O$ is not a function of X and Y. No correlation in $\delta^{18}O$ with the

distance from the edges of the calcite standard grains (NBS-18 and NBS-19) was observed. Taken together, this evidence indicates that the elevated $\delta^{18}O$ values at the edges of our experimental crystals are not an analytical artefact—i.e., they are not the result of the sub-micron relief between center and edge of the crystals.

Results

Isotopic composition of bulk calcite and fluids

The isotopic composition of the final fluid and those sub-sampled after addition of Nd, Tb, and Pr spikes was constant in the experiment conducted at 24.6°C—i.e. $^{18}O/^{16}O$ = 0.0019841, $\delta^{18}O_{SMOW}$ = -10.53±0.010 ‰ (1 s.e.), and $\delta^{18}O_{VPDB}$ = -40.15±0.010 ‰ (Table 1). In experiment DC-1, no fluid sub-samples were collected before calcite started to grow, so in this case the baseline measurement was made in a similar manner but prior to calcite nucleation. In this similar run, $\delta^{18}O_{SMOW}$ of the fluid prior nucleation (but exposed to CO_2 atmosphere) was -10.52 ‰; therefore, the isotopic composition of the fluid was considered constant over the duration of crystallization. Bulk analyses of calcite crystals having sizes >1 mm were the same as those measured by SIMS (run DC-1): $^{18}O/^{16}O$ = 0.0020416 and $\delta^{18}O_{VPDB}$ = -12.37±0.025 ‰ (the expressed uncertainties are at the 1σ level and are based on replicate analyses of fluid and calcite). The fractionation factor of $^{18}O/^{16}O$ between bulk calcite and fluid ($\alpha^{18}O$) is thus 1.02900, so $\Delta^{18}O$ = 28.58±0.027 ‰ at 24.6°C. The average of all SIMS $\Delta^{18}O$ measurements in calcite crystals from the same experiment is 28.56±0.137 ‰ (Table 2).

Over the course of run DC-1, the Ca concentration decreased in the solution but DIC, pH, and CO_3^{2-} increased (Table 1). Almost the entire size of the crystals precipitated before introduction of the Sm spike in runs DC-15, DC-3, and DSC-4 because of the fast supply of

CO_2 and consequent high growth rate. The $\delta^{18}O$ value in these runs was assumed to be equal to those in DC-1, because the same initial fluid was used in all experiments.

In situ determined fractionation factors

Oxygen isotope fractionation factors were determined for each SIMS analytical spot and are presented in the Table 2 and 3. Values of $\Delta^{18}O$ were determined at 177 spots in the six edge-to-edge profiles of three calcite crystals precipitated at 24.6°C. Forty $\Delta^{18}O$ values were characterized in the four profiles of the three crystals in other experiments. Prior SIMS analyses for REE in calcite crystals precipitated at 24.6°C demonstrated that these crystals recorded the REE pattern corresponding to the introduction of REE into growth medium. An example of SIMS-determined $\Delta^{18}O$ values across the largest calcite crystal is presented on Figure 1a. Here, oxygen isotope fractionation increases toward the edge of the crystal. The crystal zones marked with REE are also shown in Figure 1a. The appearance of REE corresponds to the sequence of its addition into fluid; i.e., starting with Sm and ending with Tb and Pr. The growth rates were determined as the width of each zone (Δx) in each profile divided by the time between REE spikes (Δt) (note that Δt values between different spikes are not equal to each other). Growth rates in the crystal interiors are higher than at the edges—that is, V decreased from 0.11 to $5.4 \cdot 10^{-3}$ nm/s in the Sm-La and Tb-Pr zones respectively (Figure 1b). The value of $\Delta^{18}O$ decreases by 1 ‰ with increasing crystal growth rate. The fractionation factor ($\alpha^{18}O$) was calculated as $\alpha^{18}O = {}^{18}O/{}^{16}O(t)_{calcite}/{}^{18}O/{}^{16}O_{fluid}$, where ${}^{18}O/{}^{16}O(t)_{calcite}$ is the averaged data from multiple SIMS spots collected in particular REE-spiked zone of the calcite, with uncertainty expressed as the standard error of these data. The growth rate, V, of a given crystal is highest at the center (the innermost zone of the crystal grown prior to addition of the Sm spike). In this region, V was estimated from the time elapsed between nucleation of visible

crystals on the wall of the beaker and addition of Sm (Table 4, prior Sm rows). Based on this approach, the initial high V values are estimated to have been at least 0.2 nm/s. Individual crystal edge-to-edge profiles, together with $\Delta^{18}O$ versus V, are presented in Figure 2 (DC-1). Fractionation generally increases from crystal center to edge, and thus has an inverse relationship with growth rate. The only exception is the left side of the profile through crystal-6 (Figure 2e).

Calcite crystals from experiments at temperatures other than 24.6°C grew mainly before addition of Sm (the first REE spike). In all cases, all REE spikes were detected only at the outermost SIMS spots at the edge of the crystals. The growth rates were estimated to be no lower than 5.8 nm/s, because crystals grew up to few hundreds of microns in size over 12 hours at 19.7 and 21.7°C. Estimation of V of calcites grown at 15°C yielded the rates of at least 0.7 nm/s. The values of $\Delta^{18}O$ within space of the individual crystals are presented in Figure 3. The largest fractionation difference (3 ‰) was observed between the edge and the center of the crystal grown at 15°C (Figure 3a). The three profiles confirm the trend observed on Figure 2 (Figure 3a,b,c), with the exception of the crystal grown at 21.7°C (DC-3, Figure 3d), in which $\Delta^{18}O$ decreases from one crystal edge to another. This inconsistency could be explained as an artefact of the specific section made through this crystal. In contrast with calcites precipitated at 24.6°C, the lack of a REE pattern in this 21.7°C crystal means there is no guarantee that nucleation occurred at the crystal center, nor that the exposed polished section represents the crystal/flask interface.

The extreme values of $\Delta^{18}O$ from centers and edges of calcite crystals are plotted against their precipitation temperature in Figure 4 (also see Table 5). Each of the plotted points is the average of the data collected at centers (diamonds) and edges (circles) of the crystals. The

largest difference of 3 ‰ occurs between edges and centers of the crystals precipitated at 15°C. The red bar represents the maximum single measurement collected at the edge of crystal 1, where $\Delta^{18}O$ = 29.79 (DC-1). The discrepant data from the rapidly-grown centers of the crystals are depleted in ^{18}O relative to the slowly-grown edges, and also relative to the temperature calibration in cave deposits reported by (Demény et al. 2010) (Figure 4). Previous experimental $\Delta^{18}O$-T°C calibrations overlap with our scattered data of the rapidly-grown calcites (O'Neil at el. 1969; Kim and O'Neil 1997). Calculated $\Delta^{18}O_{calcite-CO_2}$ reported by Chacko and Deines (2008), together with $\Delta^{18}O_{H_2O-CO_2}$ from Brenninkmeijer et al. (1983), yield $\Delta^{18}O_{calcite-H_2O}$ values that also overlap with those of our rapidly grown calcites.

Discussion

The direction of our $\Delta^{18}O$ vs. growth rate trend is consistent with results of previous studies incorporating different experimental designs and bulk (rather than *in situ*) calcite analyses (Dietzel et al. 2009; Day and Henderson 2011). The combined data from crystals grown at 24.6°C are shown in comparison with the data of Dietzel et al. (2009) in Figure 5. Their data are from experiments performed at 25°C and pH = 8.3. Bulk precipitation rates (μmol/m^2/s) were recalculated as linear growth rates (nm/s) using the molar volume of calcite (36.99 cm^3/mol). Note that this conversion assumes growth of a single crystal, not a collection of small crystals (up to 5 μm in size) such as those described by Dietzel et al. (2009). Their recalculated V could be underestimated for this reason. In both datasets $\Delta^{18}O$ approaches the calculated equilibrium calcite-fluid value of Zheng (1999) and Zeebe (2007) at slow growth rates (V<10^{-3} nm/s) and decreases toward calculated $\Delta^{18}O_{eq}(CO_3^{2-}$-fluid) at fast growth. Calculations of Zheng (1999) were performed by increment method based on cation-oxygen

bond strength and did not account changes in the fluid chemistry (also see Zheng 2011). Zebee's (2007) calculations depend on pH and were performed for T = 24.6°C, pH = 8.17 (NBS-scale), and salinity of 35 psu using the Excel spreadsheet from Zeebe's website (http://www.soest.hawaii.edu/oceanography/faculty/zeebe.html). According to these calculations, an increase in pH from 8.00 to 8.17 (the range in the experiment at 24.6°C) would decrease $\Delta^{18}O_{eq}$ by 0.1 ‰, which is insignificant because it is within SIMS analytical error.

The small change of pH in our experiment cannot explain the observed α^{18}O-V trend during calcite precipitation at 24.6°C (Table 1). The pH in our fluid increased from 7.96±0.06 to 8.17±0.02 during crystallization, but α^{18}O increases, in opposition to the trend expected from Zeebe's calculations. According to Usdowski and Hoefs (1993) and Zeebe (1999, 2007), increasing pH causes enrichment of CO_3^{2-} in the fluid, which decreases the equilibrium value of α^{18}O. Our data cannot be explained by this mechanism.

The decrease of α^{18}O with increasing V is consistent with behavior suggested by the growth entrapment model (GEM), which describes disequilibrium fractionation of elements and isotopes between a crystal and its growth medium as a consequence of the "capture" of a chemically and isotopically anomalous near-surface region of the lattice during crystal growth. In this model, the extent of fractionation is determined in part by the parameter F, which is the *equilibrium* partition coefficient (or fractionation factor) between the near-surface and the deeper lattice (whose value is unknown *a priori*) (Watson and Liang 1995; Watson 1996; Watson 2004). Partial or complete capture of the near-surface composition within the crystal further depends on the trade-off between the growth rate (which tends to "bury" the near-surface layer) and diffusion (which tends to erase the chemical anomaly). The outcome of this competition is determined by the thickness of the near-surface layer and diffusivity of the

element of interest in it. The anomalous layer owes its existence at least in part to relaxation from their normal lattice positions of atoms located within ~1 nm of the surface (see Fenter et al. 2000 and Rohl et al. 2003). Partially-formed sites at step edges on growth hillocks may also play a role (e.g., Reeder 1996), however, so the effective thickness of the near-surface anomaly is not well constrained. By analogy with diffusion along surfaces and in grain boundaries, it is inevitable that diffusion in the near-surface of a crystal is faster than "normal" lattice diffusion in the same crystal. Indeed, Stipp et al. (1992) suggested that solid state diffusion in the near-surface region (characterized by near-surface diffusivity D_s) is many orders of magnitude faster than diffusion deeper in the calcite lattice. Watson and co-workers consider that equilibrium fractionation between crystals and their growth media can occur only when D_s dominates over V: "a growing crystal assumes the composition of its [near] surface unless diffusion in the near-surface region is effective during growth". If V dominates over D_s, the anomalous surface is recorded (at least partially) in the overall composition of the crystal. If D_s is completely ineffective during growth, the composition of the resulting crystal differs from the equilibrium composition by the factor F. The growth entrapment model was used successfully to explain disequilibrium effects for minor elements and calcium isotopes fractionation between calcium carbonate minerals and fluid (Gabitov and Watson 2006; Gaetani and Cohen 2006; Gabitov et al. 2008; Tang et al. 2008a,b).

Our results suggest that the near surface region of calcite is depleted in ^{18}O relative to the lattice at equilibrium. During slow growth, our $\alpha^{18}O$ is close to the predicted equilibrium value (Zeebe 2007) and overlaps with value in slow growing cave deposit (Coplen 2007), demonstrating minimal capture of ^{18}O from the near-surface region of calcite (Figures 4 and 5). We suggest that during fast calcite growth, the low ^{18}O of the near-surface region is partially

captured by the newly formed lattice, decreasing the apparent $\alpha^{18}O$ toward $\alpha^{18}O_{eq}(CO_3^{2-}$-fluid). This implies that CO_3^{2-} is one of the major sources of ^{18}O in calcite, which is consistent with modeling and *in situ* characterization of the calcite/H_2O interface (van Cappellen et al. 1993; Stipp 1999; Fenter et al. 2000). However, in contrast to the data of Dietzel et al. (2009), our data show that even at very high growth rates $\alpha^{18}O$(lattice-fluid) is still 4 ‰ higher than $\alpha^{18}O_{eq}(CO_3^{2-}$-fluid). One potential explanation for this behavior is that V in our experiments was not high enough for 100 % capture of ^{18}O from CO_3^{2-} by the calcite lattice, whereas V from the work of Dietzel et al. (2009) is actually faster than their recalculated estimates based on the mass precipitation rate. When growth entrapment is 100% efficient, $\alpha^{18}O$(lattice-fluid) = $\alpha^{18}O_{eq}$(surface-fluid); however, it is important to note that $\alpha^{18}O_{eq}$(surface-fluid) is not necessarily equal to $\alpha^{18}O_{eq}(CO_3^{2-}$-fluid). Therefore $\alpha^{18}O$ need not approach $\alpha^{18}O_{eq}(CO_3^{2-}$-fluid) at very high V. Note, in addition, that only one datum of Dietzel et al. (2009) is close to $\alpha^{18}O_{eq}(CO_3^{2-}$-fluid). In this case $\alpha^{18}O_{eq}$(surface-fluid) is in between $\alpha^{18}O_{eq}$(calcite-fluid) and $\alpha^{18}O_{eq}(CO_3^{2-}$-fluid).

A second possible explanation of our gentle $\alpha^{18}O$-V slope relative to that of Dietzel et al. (2009) is the constant flux of isotopically distinct CO_2 into the fluid. It is possible that there was insufficient time in our experiments for equilibration of ^{18}O between aqueous carbonate species and fluid, which resulted in capture of non-equilibrium elevated ^{18}O composition of CO_3^{2-} by fast-growing calcite. Aqueous carbonate anion that failed to equilibrate with fluid would be enriched in ^{18}O from its primary source – ammonium carbonate. [Note that $\delta^{18}O$ of the initial fluid—prior to contact with CO_2 atmosphere—was lower than $\delta^{18}O$ of the calcite growth medium by 0.2±0.05 ‰ (i.e. analytical uncertainty is 25 %)]. This explanation is consistent with the findings of Beck et al. (2005) for the witherite-fluid system, where 2-3

hours are required to reach equilibrium in $\delta^{18}O$ fractionation between carbonate species and H_2O. Our fast growth rates (V>0.2 nm/s) produce a few μm layer of calcite during that time, which is thick enough to contribute in $\delta^{18}O$ of the 20-30 μm spot analysis. Slow growing calcite should not be affected by CO_3^{2-}-H_2O disequilibrium.

A final alternative explanation is that rapid "consumption" of CO_3^{2-} (not equilibrated with HCO_3^-) might retain signatures from the ^{18}O-rich HCO_3^-, leading to elevation of $\alpha^{18}O$ at high V. This explanation is consistent with the interpretation of O'Neil (1969) and also with observations from natural hot-spring travertines by Kele et al. (2011). Surprisingly, the disequilibrium value of $\alpha^{18}O$ resolved from the temperature calibration of rapidly precipitated (10 nm/s) travertines (Kele et al. 2008 and 2011) is consistent with $\alpha^{18}O$ of our slowly grown calcites at 24.6°C. This consistency may result from rapid CO_3^{2-} "consumption" during travertine calcite growth as discussed above. In addition, the crystallization of travertines is complicated by other processes, including evaporation and CO_2 degassing, which probably cannot be ruled out with semi annual sub-sampling and analyzing $\delta^{18}O$ and chemistry of the fluids (see Kele et al. 2008).

In closing this discussion of the underlying cause of non-equilibrium behavior during calcite growth, it is important to note that the growth entrapment model (Watson 2004) is not the only possible explanation for non-equilibrium uptake of isotopes. DePaolo (2011) attributes the phenomenon entirely to surface reaction kinetics that depend on isotope identity. Contributions from such an effect are certainly possible, but the DePaolo model does not consider the well-established fact that the atomic structure of calcite and other minerals differs from that of the bulk lattice to distances of ~1 nm from the surface (e.g., Fenter 2000). Exchange of atoms within this near-surface layer must involve site-to-site jumps, and is

therefore, in our opinion, best described as diffusion. The inability of diffusion within this layer to maintain equilibrium during growth is the essence of the growth entrapment model.

The lack of temperature dependence of $\alpha^{18}O$ from the centers of calcite crystals confirms the existence of non-equilibrium ^{18}O fractionation between fast growing calcite and fluid (Figure 4). The overlap of our disequilibrium data with previous experimental calibrations (O'Neil at el. 1969; Kim and O'Neil 1997) suggests that calcites may not have grown at equilibrium in these earlier experiments. The isotopic composition of our slowly grown crystal edges represents conditions close to equilibrium. The fit from our work yields the following equation:

$$\Delta^{18}O = 17746/T-30.238$$

where T is in Kelvin and $r^2=0.97$. This equation is based on our crystal edges grown slowly at the temperature range from 15 to 25°C. Our maximum crystal-edge $\alpha^{18}O$ overlaps with those from slowly grown (10^{-5} nm/s) cave deposits reported by Coplen (2007), representing the maximum and closest to equilibrium experimentally determined $\alpha^{18}O$ at 25°C.

Conclusions

The data obtained in this study provide the first evidence from *in situ* analyses that high growth rate of individual crystals causes depletion of ^{18}O in the calcite lattice. At slow growth rates, $\alpha^{18}O$ measured in the same crystals approaches accepted equilibrium values. Our maximum $\Delta^{18}O$ value of 29.79±0.14 ‰ together with our calibration curve are the closest to the calculated equilibrium fractionation in experimental data from the literature on calcites grown at 25°C. Non-equilibrium ^{18}O fractionation between rapidly grown calcite and fluid masks the temperature dependence. The highest discrepancy of 3 ‰ between fast- and slow-growing calcite is observed at 15°C suggesting an increase in the effectiveness of growth entrapment,

perhaps due to slower diffusion in the near-surface layer at low temperature. $\alpha^{18}O$ decreases with increasing crystal growth rate toward $\alpha^{18}O_{eq}(CO_3^{2-}\text{-fluid})$ but does not actually reach this value. Therefore isotopic exchange between aqueous CO_3^{2-} and HCO_3^- partially affects apparent $\alpha^{18}O$ during disequilibrium (rapid) calcite growth.

Acknowledgments. We would like to thank Axel Schmitt, Kevin McKeegan, and Mark Harrison for their help and support with the ion microprobe measurements. Experiments and SIMS analyses were supported by U.S. NSF, EAR, Instrumentation and Facilities Program. We also thank Howard Spero for fluid $\delta^{18}O$ analyses, which were covered by NSF grant no. EAR-0738843 to EBW. We are grateful to Aleksey Sadekov, Walter Geibert, and ICP-OES laboratory at the University of Edinburgh for support in fluid Ca analyses. We thank Anita Leinweber for measuring DIC; these analyses were covered by ETH grant no. 4 443869-AL-20600. We also thank the Editor-in-Chief Uwe Brand, Sándor Kele, and an anonymous reviewer for their comments on the manuscript.

References

Baker A., Genty D., Dreybrodt W., Barnes W.L., Mockler N.J., and Grapes J. (1998) Testing theoretically predicted stalagmite rate with recent annually laminated samples: Implications for past stalagmite deposition. *Geochim. Cosmochim. Acta*, **62**, 393-404.

Barras C., Duplessy J.-C., Geslin E., Michel E., and Jorissen F.J. (2010) Calibration of $\delta^{18}O$ of cultured benthic foraminiferal calcite as a function of temperature. *Biogeosc*., **7**, 1349–1356.

Beck W.C., Grossman E.L., and Morse, J.W. (2005) Experimental studies of oxygen isotope fractionation in the carbonic acid system at 15°, 25°, and 40°C. *Geochim. Cosmochim. Acta*, **69**, 3493-3503.

Bentov S. and Erez J. (2006) Impact of biomineralization processes on the Mg content of foraminiferal shells: a biological perspective. *Geochem. Geophys. Geosyst*., **7**, Q01P08. doi:10.1029/2005GC001015.

Brenninkmeijer C. A. M., Kraft P., and Mook W. G. (1983) Oxygen isotope fractionation between CO_2 and H_2O. *Chem. Geol. (Isot. Geosc. Sect.)* **1,** 181–190.

Broecker W. S. (1986) Oxygen isotope constraints on surface ocean temperatures. *Quat. Res.* **26,** 121-134.

Chacko T. and Deines P. (2008) Theoretical calculation of oxygen isotopic fractionation factors in carbonate systems. *Geochim. Cosmochim. Acta*, **72**, 3642–3660.

Coplen (2007) Calibration of the calcite–water oxygen-isotope geothermometer at Devils Hole, Nevada, a natural laboratory. *Geochim. Cosmochim. Acta*, **71**, 3948–3957.

Day C.C. and Henderson G.M. (2011) Oxygen isotopes in calcite grown under cave-analogue conditions. *Geochim. Cosmochim. Acta*, **75**, 3956–3972.

Demény A., Kele S., and Siklósy Z. (2010) Empirical equations for the temperature dependence of calcite-water oxygen isotope fractionation from 10 to 70°C. *Rapid Commun. Mass Spectrom*, **24**, 3521–3526.

DePaolo D.J. (2011) Surface kinetic model for isotopic and trace element fractionation during precipitation of calcite from aqueous solutions Source. *Geochim. Cosmochim. Acta*, **75**, 1039-1056.

Dickson A. G. and Millero F. J. (1987) A comparison of the equilibrium constants for the dissociation of carbonic acid in seawater media. , *Deep-Sea Research*, ***34***, 1733-1743.

Dietzel M., Tang J. W., Leis A., and Kohler S. J. (2009) Oxygen isotopic fractionation during inorganic calcite precipitation - Effects of temperature, precipitation rate and pH. *Chem. Geol.*, **268**, 107-115.

Epstein S., Buchsbaum R., Lowenstam H. A., and Urey H. C. (1953) Revised carbonate-water isotopic temperature scale. *Geol. Soc. Am. Bull.* **64,** 1315–1325.

Erez J. (2003) The source of ions for biomineralization in foraminifera and their implications for paleoceanographic proxies. In: Biomineralization (eds. P.M. Dove, J.J. De Yoreo and S. Weiner). *Rev. Mineral. Geochem*., **54**, 115–149.

Fayek M., Harrison T. M., Ewing R. C., Grove M., and Coath C. D. (2002) O and Pb isotopic analyses of uranium minerals by ion microprobe and U-Pb ages from the Cigar Lake Deposit. *Chem. Geol.* **185,** 205–225.

Fenter P., Geissbuhler P., Dimasi E., Srajer J., Sorensen L.B., and Sturchio N.C. (2000) Surface speciation of calcite observed in situ by high-resolution X-ray reflectivity**.** *Geochim. Cosmochim. Acta*, **64**, 1221-1228.

Freitas P.S., Clarke L.J., Kennedy H., and Richardson C.A. (2008) Inter- and intra-specimen variability masks reliable temperature control on shell Mg/Ca ratios in laboratory- and field-cultured Mytilus edulis and Pecten maximus (bivalvia). *Biogeosc.,* **5,** 1245-1258.

Friedman I., O'Neil J., and Cebula G. (1982) Two New Carbonate Stable-Isotope Standards. *Geostand. Newslett.,* **6**, 11-12.

Gabitov R.I. and Watson E.B. (2005) Preliminary experimental results for ^{18}O and ^{13}C uptake in calcite and at 32°C and various precipitation rates. *Geochim. Cosmochim. Acta,* **69**, 10, A777.

Gabitov R.I. and Watson E.B. (2006) Partitioning of strontium between calcite and fluid. *Geochem. Geophys. Geosys.* **7**, Q11004, doi:10.1029/2005GC001216.

Gabitov R. I., Gaetani G. A., Watson E. B., Cohen A. L. and Ehrlich H. L. (2008) Experimental determination of temperature and growth rate effects on U^{6+} and Mg^{2+} partitioning between aragonite and fluid. *Geochim. Cosmochim. Acta,* **72**, 4058–4068.

Gaetani G.A. and Cohen A.L. (2006) Element partitioning during precipitation of aragonite from seawater: A framework for understanding paleoproxies. *Geochim. Cosmochim. Acta,* **70**, 4617-4634.

Grinstein M., Bentov S., Koller-Rink S., De Beer D., and Erez J. (2004) Direct microelectrodes measurements at the calcification site of foraminifera. *EOS Trans. AGU*, Fall Meet. San Francisco. #B21B-0864 (abstr.).

Gruzensky P.M. (1967) Growth of calcite crystals. *J. Phys. Chem. Solids,* S **1**, 365-367.

Johnson K. M., Wills K. D., Buttler D. B., Johnson W. K. and Wong C. S. (1993) Coulometric total carbon dioxide analysis for marine studies: maximizing the performance of an automated gas extraction system and coulometric detector. *Mar. Chem*., **44**, 167-187.

Kele S., Demény A., Siklósy Z., Németh T., Tóth M., and Kovács M.B. (2008) Chemical and stable isotope composition of recent hot-water travertines and associated thermal waters, from Egerszalók, Hungary: Depositional facies and non-equilibrium fractionation. *Sed. Geol.*, **211**, 53–72.

Kele S., Özkul M, Fórizs I. , Gökgöz, A., Baykara M.O., Alçiçek, M.C., and Németh T. (2011) Stable isotope geochemical study of Pamukkale travertines: New evidences of low-temperature non-equilibrium calcite-water fractionation. *Sed. Geol.*, **238**, 191–212.

Kim S.-T. and O'Neil J.R. (1997) Equilibrium and nonequilibrium oxygen isotope effects in synthetic carbonates. *Geochim. Cosmochim. Acta*, **61**, 3461-3475.
Labeyrie L. D., Duplessy J.-C., and Blanc P. L. (1987) Variations in mode of formation and temperature of oceanic deep waters over the past 125,000 years. *Nature* **327,** 477-482.

Kita N.T., Ushikubo T., Fu B., Valley J.W. (2009) High precision SIMS oxygen isotope analysis and the effect of sample topography. *Chem. Geol.*, **264**, 43–57.

Lea D.W., Pak D.K., and Spero H.J. (2000) Climate Impact of Late Quaternary Equatorial Pacific Sea Surface TemperatureVariations. *Science*, **289**, 1719-1724.

Lewis E. and D. W. R. Wallace (1998), *Program developed for CO2 system calculations.*, Carbon Dioxide Information Analysis Center, Oak Ridge National Laboratory, U.S Department of Energy, Oak Ridge, Tennessee.

Lorens R.B. (1981) Sr, Cd, Mn, and Co distribution coefficients in calcite as a function of calcite precipitation rate. *Geochim. Cosmochim. Acta*, **45**, 553-561.

O'Neil J.R., Clayton R.N., and Mayeda T.K. (1969) Oxygen isotope fractionation in divalent metal carbonates. *J. Chem. Phys*., **51**, 5547–5558.

Owen, R., Kennedy, H., and Richardson, C. (2002) Isotopic partitioning between scallop shell calcite and seawater: Effect of shell growth rate. *Geochim. Cosmochim. Acta*, **66**, 1727-1737.

Reeder J.R. (1996) Interaction of divalent cobalt, zinc, cadmium, and barium with the calcite surface during layer growth. *Geochim. Cosmochim. Acta*, **60**,1543-1552.

Rohl A.L., Wright K., and Gale J.D. (2003) Evidence from surface phonons for the (2x1) reconstruction of the (101–4) surface of calcite from computer simulation. *Am. Mineral. (Letters), **88**, 921–925.*

Rollion-Bard C., Erez J., and Zilberman T. (2008) Intra-shell oxygen isotope ratios in the benthic foraminifera genus Amphistegina and the influence of seawater carbonate chemistry and temperature on this ratio. *Geochim. Cosmochim. Acta*, **72**, 6006–6014.

Stipp, S.L.S., Hochella Jr., M.F., Parks, G.A., and Leckie, J.O. (1992) Cd^{2+} uptake by calcite, solid-state diffusion, and the formation of solid-solution: Interface process observed with near-surface sensitive techniques (XPS, LEED, and AES). *Geochim. Cosmochim. Acta*, **56**, 1941-1954.

Stipp S.L.S. (1999) Toward a conceptual model of the calcite surface: Hydration, hydrolysis, and surface potential. *Geochim. Cosmochim. Acta*, **63,** 3121–3131.

Stoll H.M., Rosenthal Y., and Falkowski P. (2002) Climate proxies from Sr/Ca of coccolith calcite: Calibrations from continuous culture of *Emiliania huxleyi*. *Geochim. Cosmochim. Acta*, **66**, 927–936.

Tang J., Köhler, S.J., and Dietzel, M. (2008a) Sr^{2+}/Ca^{2+} and $^{44}Ca/^{40}Ca$ fractionation during inorganic calcite formation: I. Sr incorporation. *Geochim. Cosmochim. Acta*, **72**, 3718-3732.

Tang J., Dietzel M., Bohm F., Kohler S.J., and Eisenhauer A. (2008b) Sr^{2+}/Ca^{2+} and $^{44}Ca/^{40}Ca$ fractionation during inorganic calcite formation: II. Ca isotopes. *Geochim. Cosmochim. Acta*, **72**, 3733-3745.

Tesoriero, A.J. and Pankow, J.F. (1996) Solid solution partition of Sr^{2+}, Ba^{2+}, and Cd^{2+} to calcite. *Geochim. Cosmochim. Acta*, **60**, 1053-1063.

ter Kuile B. and Erez J. (1984) In situ growth rate experiments on the symbiotic-bearing foraminifera. *Amphisteginalobifera* and *Amphisorushemprichii*. *J. Foram. Res.*, **14**, 262-276.

Usdowski E. and Hoefs J. (1993) Oxygen isotope exchange between carbonic acid, bicarbonate, carbonate, and water: a re-examination of the data of McCrea (1950) and an expression for the overall partitioning of oxygen isotopes between the carbonate species and water. *Geochim. Cosmochim. Acta*, **57**, 3815–3818.

van Cappellen P., Charlet L., Stumm W., and Wersin P. (1993) A surface complexion model of the carbonate mineral-aqueous solution interface. *Geochim. Cosmochim. Acta*, **57,** 3505–3518.

Watson, E.B. and Liang, Y. (1995) A simple model for sector zoning in slowly growing crystals: Implications for growth rate and lattice diffusion, with emphasis on accessory minerals in crustal rocks. *Am. Mineral.*, **80**, 1179-1187.

Watson, E.B. (1996) Surface enrichment and trace-element uptake during crystal growth. *Geochim. Cosmochim. Acta*, **60**, 5013-5020.

Watson, E.B. (2004) A conceptual model for near-surface kinetic controls on the trace-element and stable isotope composition of abiogenic calcite crystals. *Geochim. Cosmochim. Acta*, **68**, 1473-1488.

Zeebe R.E. (1999) An explanation of the effect of seawater carbonate concentration on foraminiferal oxygen isotopes. *Geochim. Cosmochim. Acta*, **63**, 2001–2007.

Zeebe R.E. (2007) An expression for the overall oxygen isotope fractionation between the sum of dissolved inorganic carbon and water", Geochem., Geophys., Geosys., **8**, 9, Q09002, doi:10.1029/2007GC001663.

Zheng Y-F. (1999) Oxygen isotope fractionation in carbonate and sulfate minerals. *Geochem. J.*, **33**, 109-126.

Zheng Y-F. (2011) On the theoretical calculations of oxygen isotope fractionation factors for carbonate-water systems. *Geochem. J.*, **45**, 341-354.

Zhong S. and Mucci A. (1995) Partitioning of rare earth elements (REEs) between calcite and seawater solutions at 25°C and 1 atm, and high dissolved REE concentrations. *Geochim. Cosmochim. Acta*, **59**, 443–453.

Figure Captions

Figure 1. SIMS data from the run DC-1 (crystal-1, profile-3) conducted at 24.6°C. a) An example of $\Delta^{18}O$ profile across REE-spiked calcite crystal; (b) An example of $\Delta^{18}O$ plotted versus calcite growth rate. Here the single data points are the averages of SIMS spots collected in each REE spiked zone. $\Delta^{18}O=10^3 \cdot \ln(\alpha^{18}O)$

Figure 2. $\Delta^{18}O$ profiles within the single crystals: Run at T=24.6°C. a-d) $\Delta^{18}O$ plotted versus distance from the one crystal edge to the opposite one. e) $\Delta^{18}O$ from the one crystal corner to the opposite one. f-j) $\Delta^{18}O$ plotted versus calcite growth rate, determined similarly as on the Figure 1. REE pattern showed that nucleation occurred around the center of each crystal. $\Delta^{18}O=10^3 \cdot \ln(\alpha^{18}O)$

Figure 3. $\Delta^{18}O$ profiles within the single crystals: Runs at T=15, 19.7, and 21.7°C. a-b) two crystals grown at 15°C; c-d) two crystals grown at 19.7 and 21.7°C respectively. REE pattern was not preserved by the crystals, therefore, crystals centers do not necessarily correspond to their nucleation. $\Delta^{18}O=10^3 \cdot \ln(\alpha^{18}O)$

Figure 4. Effect of calcite growth rate and temperature on $\Delta^{18}O=10^3 \cdot \ln(\alpha^{18}O)$. Circles and diamonds are the averaged data from the edges and the center of the multiple crystals respectively. Triangle is the datum of Coplen (2007) from cave deposits extrapolated to 24.6 from 33.7°C using the slope of 0.0002 K^{-1}. Bar is the maximum datum is from the edge of the Crystal-1 (profile 1). Dark red dash line is based on calculations of Chacko and Deines (2008). Blue dash-dot and black solid and lines are the calibrations from the experimental work of O'Neil et al. (1969) and Kim and O'Neil (1997) respectively. Brown dot line represents data from cave deposits (Demény et al., 2010). Red line is the fit of our data from the slow grown edges of the crystals. Green solid line is based on modeling results of Zeebe (2007).

Figure 5. Dependence of $\Delta^{18}O$ on growth rate at 24.6°C: Comparison with literature data. Solid circles are the data from three profiles from the Crystal-1. Diamonds and triangles and are the data from the single profiles from the Crystals 2 and 6 respectively. The empty circles are from Dietzel et al. (2009). The dashed lines are the calculations based on Zeebe (2007). The growth rates for the data inside the box are from the core of the Crystal-1 and were estimated as no less than 0.2 nm/s. $\Delta^{18}O=10^3 \cdot \ln(\alpha^{18}O)$

Table 1. Composition of the sampled fluids from which calcite grew at 24.6°C (DC-1).

sub-sample	t days	Ca ppm	pH (NBS)	DIC µmol/kg	CO_3^{2-} µmol/kg	Ω	$\delta^{18}O_{SMOW}$ ‰
Initial	-43	327.3	5.5	low	low	low	-10.72
Nd-spike	35.8	157.5	8.06	2410	192.1	1.75	-10.54
Tb-spike	85.9	143.9	8.15	2685	258.9	2.14	-10.53
Pr-spike	129.0	n/a	8.16	n/a	n/a	n/a	-10.50
Final	149.9	95.2	8.17	2775	279.0	1.55	-10.55

t is the time of crystallization from the addition of Sm spike.
Ω is the fluid saturation state with respect to calcite.
Initial time was estimated as 43 days prior Sm addition by visual monitoring of the experimental flask with naked eye every 1-8 days. The onset of calcite precipitation was assumed to occur at -8<t<0 days.
Sm, Nd, and Tb correspond to the fluid sub-sample collected just before addition of REE.
DIC is the dissolved inorganic carbon.
CO_3^{2-} and Ω calculations were performed using an excel implementation of CO2SYS (Lewis and Wallace 1998), modified to use measured calcium concentrations. The constants of Dickson and Millero (1987) were used for the carbonate and sulfate system respectively. Please note that sulfur was not added to our laboratory prepared solution.
Initial fluid was not exposed to CO_2 atmosphere. Fluid $\delta^{18}O$ during crystallization was constant and equal to $\delta^{18}O_{SMOW}$ = -10.53±0.010 ‰ (1 s.e.), and $\delta^{18}O_{VPDB}$ = -40.15±0.010 ‰. $\delta^{18}O_{SMOW}$ during exposure to CO_2 atmosphere but prior nucleation was -10.52 ‰ in the different but similar run, therefore isotopic composition of the fluid was considered constant over duration of crystallization.
pH of the fluid at the onset of crystallization was estimated to be 7.96±0.06, which is the average of pH values at t=-8 and t=0 days.
Finnigan MAT 251 IRMS 1σ=0.05 ‰ for $\delta^{18}O_{SMOW}$.
ICP-OES instrumental 1σ=0.2 % for Ca, dilution error 2%.

Table 2. Fractionation factors of $^{18}O/^{16}O$ within single REE-spiked calcite crystals grown at 24.6°C (DC-1). SIMS profiles between the edges of the crystals.

L (μm)	$\Delta^{18}O$ (‰)	s.e.	L (μm)	$\Delta^{18}O$ (‰)	s.e.	L (μm)	$\Delta^{18}O$ (‰)	s.e.
Slow, Crystal-1, Profile-1			Slow, Crystal-1, Profile-2			Slow, Crystal-1, Profile-3		
25	29.22	0.12	15	28.77	0.12	15	29.71	0.15
66	28.91	0.11	56	28.83	0.13	51	29.34	0.17
107	28.56	0.12	97	28.49	0.13	92	29.05	0.14
148	28.33	0.11	138	28.44	0.12	133	29.29	0.14
189	28.50	0.13	179	28.73	0.13	174	28.85	0.15
230	28.29	0.13	220	28.24	0.11	215	28.66	0.14
271	28.27	0.10	261	28.09	0.11	256	28.69	0.14
312	28.34	0.10	302	28.11	0.13	297	28.37	0.16
353	28.73	0.12	343	27.80	0.11	338	28.48	0.14
394	28.51	0.12	385	27.68	0.11	388	28.22	0.13
435	28.24	0.13	436	28.41	0.13	429	28.63	0.14
476	28.52	0.13	477	28.23	0.11	479	28.55	0.15
517	28.27	0.11	518	27.93	0.12	521	28.03	0.16
558	28.25	0.12	559	28.46	0.12	562	28.34	0.15
599	27.79	0.11	601	28.55	0.11	607	28.72	0.14
640	27.78	0.13	642	28.49	0.10	648	27.73	0.16
681	28.28	0.11	683	28.04	0.12	689	27.41	0.15
726	28.74	0.12	776	27.28	0.10	730	28.02	0.15
841	29.07	0.12	876	28.15	0.10	771	27.57	0.15
882	28.30	0.12	917	27.93	0.12	821	29.13	0.16
923	28.37	0.15	958	28.11	0.11	863	28.41	0.15
964	28.63	0.12	999	27.86	0.11	913	28.30	0.16
1005	28.48	0.13	1040	27.98	0.10	963	28.31	0.14
1046	28.53	0.11	1131	28.13	0.11	1004	29.17	0.14
1087	28.84	0.13	1176	28.28	0.11	1045	28.32	0.13
1132	28.67	0.11	1217	28.15	0.12	1086	28.85	0.14
1172	28.71	0.10	1258	28.40	0.12	1128	28.79	0.15
1213	28.76	0.12	1300	28.37	0.13	1169	28.81	0.14
1254	28.85	0.10	1350	28.23	0.11	1211	29.57	0.13
1295	28.64	0.12	1408	28.24	0.11	1252	29.15	0.14
1340	28.67	0.10	1449	28.38	0.11	1293	29.35	0.14
1381	28.75	0.11				1335	29.42	0.13
1426	28.89	0.12				1376	29.78	0.14
1467	29.13	0.12				1417	29.44	0.14
						1458	29.94	0.14
						1500	29.03	0.14

SIMS analyses were performed as profiles between the edges of the crystals. For example distance L of 25 and 1467 μm corresponds to the opposite edges of the crystal, i.e. start and end of analytical profile.
The average of all $\Delta^{18}O$ values presented in this table is 28.56±0.137 ‰, which is consistent with $\Delta^{18}O$ determined in the bulk calcite using conventional mass spectrometry where $\Delta^{18}O$ =28.58±0.027 ‰.
$\alpha^{18}O=(^{18}O/^{16}O)_{calcite}/(^{18}O/^{16}O)_{fluid}$, where $(^{18}O/^{16}O)_{fluid}=0.0019841$; $\Delta^{18}O=10^3 \cdot \ln(\alpha^{18}O)$; s.e.=s.d./√n

Table 2 (continue)

L (μm)	$\Delta^{18}O$ (‰)	s.e.	L (μm)	$\Delta^{18}O$ (‰)	s.e.	L (μm)	$\Delta^{18}O$ (‰)	s.e.
Slow, Crystal-1, Profile-5			Slow, Crystal-2			Slow, Crystal-6		
70	29.28	0.13	25	29.03	0.14	30	28.55	0.16
125	28.88	0.15	66	28.94	0.15	74	28.02	0.14
175	29.61	0.13	107	28.72	0.14	118	28.20	0.13
225	29.51	0.15	149	28.33	0.15	162	28.32	0.16
275	29.35	0.14	190	28.63	0.15	206	28.11	0.13
330	29.15	0.14	232	28.24	0.16	251	28.49	0.14
386	29.27	0.14	273	28.27	0.14	295	28.17	0.15
436	29.89	0.14	315	28.05	0.14	340	28.08	0.14
491	29.52	0.14	356	28.2	0.15	385	28.62	0.16
541	28.34	0.14	398	28.49	0.14	430	28.46	0.15
591	27.84	0.13	440	27.67	0.17	475	28.03	0.16
641	28.78	0.15	482	28.18	0.15	520	27.64	0.14
691	28.38	0.14	524	27.66	0.15	565	28.64	0.15
783	28.66	0.13	566	28.15	0.13	610	28.23	0.17
894	29.23	0.15	608	28.64	0.16	655	28.47	0.14
944	29.25	0.13	650	27.96	0.16	700	28.27	0.14
994	29.00	0.16	692	28.37	0.15	745	28.46	0.14
1044	29.29	0.16	734	28.11	0.16	790	28.63	0.13
1094	29.23	0.16	776	28.61	0.14	835	28.43	0.15
1144	29.29	0.14	818	28.62	0.15	880	28.08	0.14
1194	29.39	0.14	860	28.65	0.13	925	27.74	0.16
1244	29.45	0.13	902	28.16	0.14	970	27.82	0.16
1294	29.79	0.16	944	28.3	0.15	1015	28.00	0.15
			986	28.84	0.14	1060	28.68	0.16
						1105	28.80	0.15
						1150	28.52	0.14
						1195	28.39	0.15
						1241	28.75	0.16
						1286	29.24	0.16
						1330	28.76	0.14

Table 3. Fractionation factors of $^{18}O/^{16}O$ within single calcite crystals grown at different temperatures. SIMS profiles between the edges of the crystals.

L (μm)	$\Delta^{18}O$ (‰)	s.e.	L (μm)	$\Delta^{18}O$ (‰)	s.e.
DC-15, Crystal-1, T=15°C			DC-15, Crystal-2, T=15°C		
20	30.89	0.072	20	31.27	0.15
70	30.08	0.14	65	30.77	0.10
120	30.06	0.11	110	30.35	0.10
170	28.73	0.11	155	29.59	0.10
220	29.35	0.10	200	28.25	0.11
270	30.02	0.10	250	29.93	0.13
320	31.48	0.10	295	31.05	0.12
			336	31.12	0.08
			376	30.24	0.10
DSC-4, T=19.7°C			DC-3, T=21.7°C		
20	29.65	0.11	20	29.61	0.11
70	28.92	0.090	65	29.06	0.063
120	29.44	0.071	109	29.40	0.10
170	29.34	0.10	154	30.12	0.086
220	29.00	0.11	199	29.44	0.10
270	28.18	0.069	244	29.27	0.075
320	29.14	0.080	288	28.66	0.11
370	30.19	0.11	333	28.74	0.10
420	29.66	0.082	378	28.90	0.081
470	30.10	0.088	422	28.52	0.093
			467	29.29	0.095
			512	28.49	0.10
			557	28.93	0.082
			601	28.61	0.11

$\Delta^{18}O=10^3 \cdot \ln(\alpha^{18}O)$

Table 4. Mean fractionation factors of $^{18}O/^{16}O$ in each REE-spiked zone of calcite crystals grown at 24.6°C (DC-1).

REE	V (nm/s)	s.e.	$\Delta^{18}O$ (‰), mean	s.e.
		Crystal-1, Profile-1		
Nd-Tb	0.039	$2.9 \cdot 10^{-3}$	28.73	0.15
La-Nd	0.12	$6.5 \cdot 10^{-3}$	28.57	0.11
Sm-La	0.10	$9.61 \cdot 10^{-3}$	28.55	0.09
prior Sm	≥0.34	n/a	28.36	0.14
		Crystal-1, Profile-2		
Nd-Tb	0.041	$8.7 \cdot 10^{-3}$	28.64	0.11
La-Nd	0.11	$6.5 \cdot 10^{-3}$	28.40	0.10
Sm-La	0.13	$9.6 \cdot 10^{-3}$	28.27	0.18
prior Sm	≥0.23	n/a	28.28	0.12
		Crystal-1, Profile-3		
Tb-Pr	$< 5.4 \cdot 10^{-3}$	n/a	29.47	0.47
Nd-Tb	0.045	$6.3 \cdot 10^{-3}$	29.32	0.27
La-Nd	0.11	$6.5 \cdot 10^{-3}$	28.86	0.36
Sm-La	0.11	$9.61 \cdot 10^{-3}$	28.54	0.17
prior Sm	≥0.27	n/a	28.17	0.21
		Crystal-1, Profile-5		
Nd-Tb	0.041	$3.99 \cdot 10^{-3}$	29.40	0.21
La-Nd	0.089	$6.48 \cdot 10^{-3}$	29.43	0.12
Sm-La	0.086	$9.61 \cdot 10^{-3}$	29.32	0.11
prior Sm	≥0.25	n/a	28.53	0.19
		Crystal-2		
Nd-Tb	0.049	$3.15 \cdot 10^{-3}$	28.57	0.13
La-Nd	0.14	$1.73 \cdot 10^{-2}$	28.33	0.16
		Crystal-6		
Tb-Pr	0.013	$4.0 \cdot 10^{-3}$	29.01	0.24
Nd-Tb	0.063	$4.4 \cdot 10^{-4}$	28.60	0.10
La-Nd	0.18	$1.8 \cdot 10^{-3}$	28.22	0.13

$\Delta^{18}O = 10^3 \cdot \ln(\alpha^{18}O)$

REE shows the calcite zone grew between additions of two REE spikes. For example Nd-Tb means that growth rate and fractionation factor presented in this row were determined in the calcite grown between addition of Nd and Tb spikes. The error at 1σ level is the standard error of $\Delta^{18}O$ from the multiple spots in each REE spiked zone. Growth rates from "prior Sm" zones were estimated from the times when crystals became observable in the flask and addition of Sm spike. V is less than $5.4 \cdot 10^{-3}$ in the Tb-Pr zone from Profile-3 of Crystal-1 because the size of the beam propagates V-error that exceeds the growth rate value. The V uncertainties from the identical REE-spiked zones located at opposite sides of the crystal were calculated as 1s.e. between two values of V. For example the maximum discrepancy was observed between two La-Nd spiked zones in the crystal-2, where uncertainty of $1.73 \cdot 10^{-2}$ (25 %) was calculated between V values of 0.121 and 0.156 nm/s.

Table 5. Fractionation factors of $^{18}O/^{16}O$ in centers and edges of calcite crystals grown at different temperatures.

run	T°C	$\Delta^{18}O$ (‰) centers	s.e.	$\Delta^{18}O$ (‰) edges	s.e.
DC-15	15	28.49	0.24	31.38	0.11
DSC-4	19.7	28.17	0.070	30.19	0.11
DC-3	21.7	28.49	0.10	30.12	0.090
DC-1	24.6	27.59	0.087	29.33	0.18

$\Delta^{18}O=10^3 \cdot \ln(\alpha^{18}O)$

Fractionation factors determined in the centers of calcite crystals correspond to the fast calcite growth rate in contrast to the edges, which grew slower.

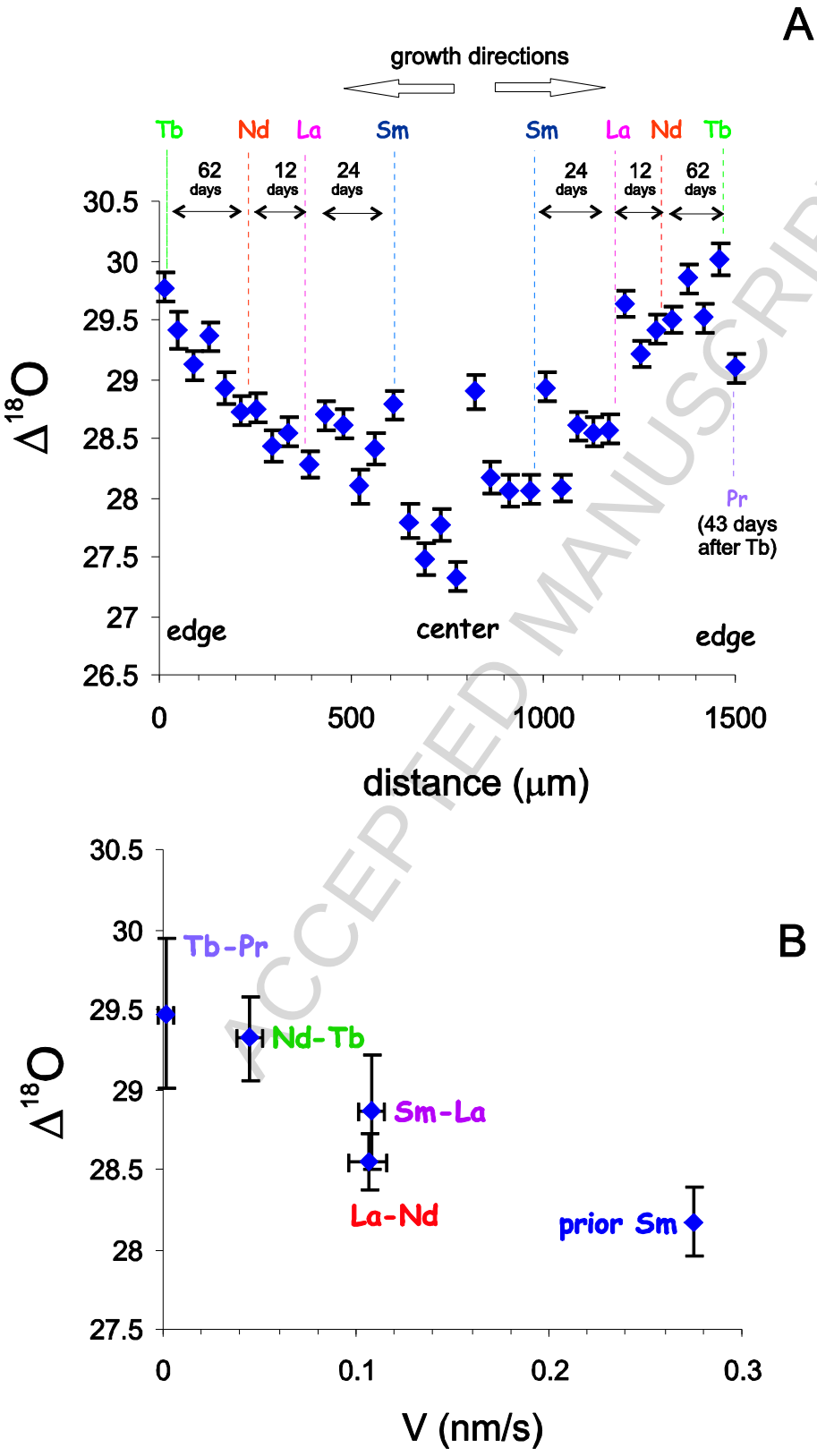

Figure 1

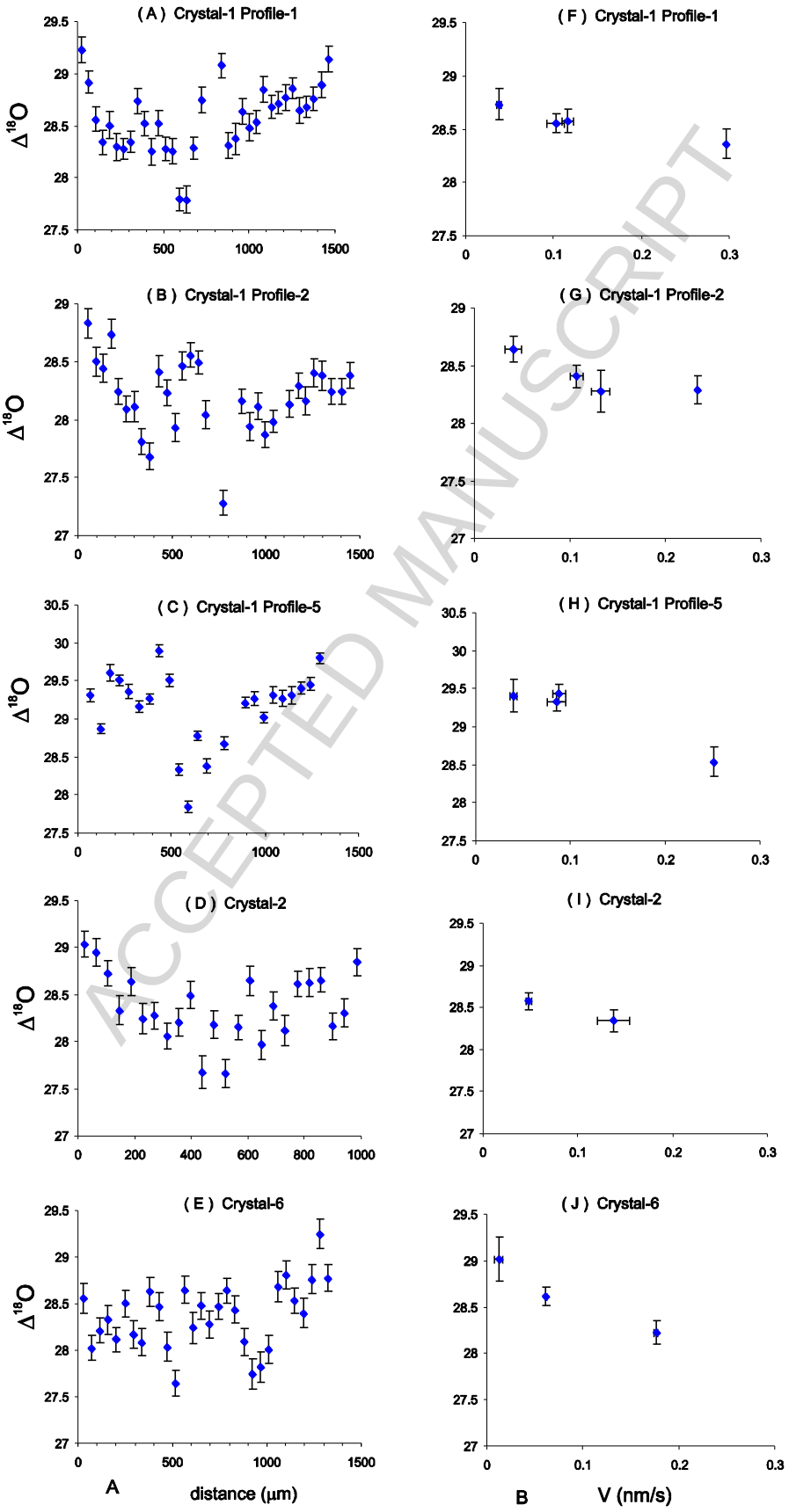

Figure 2

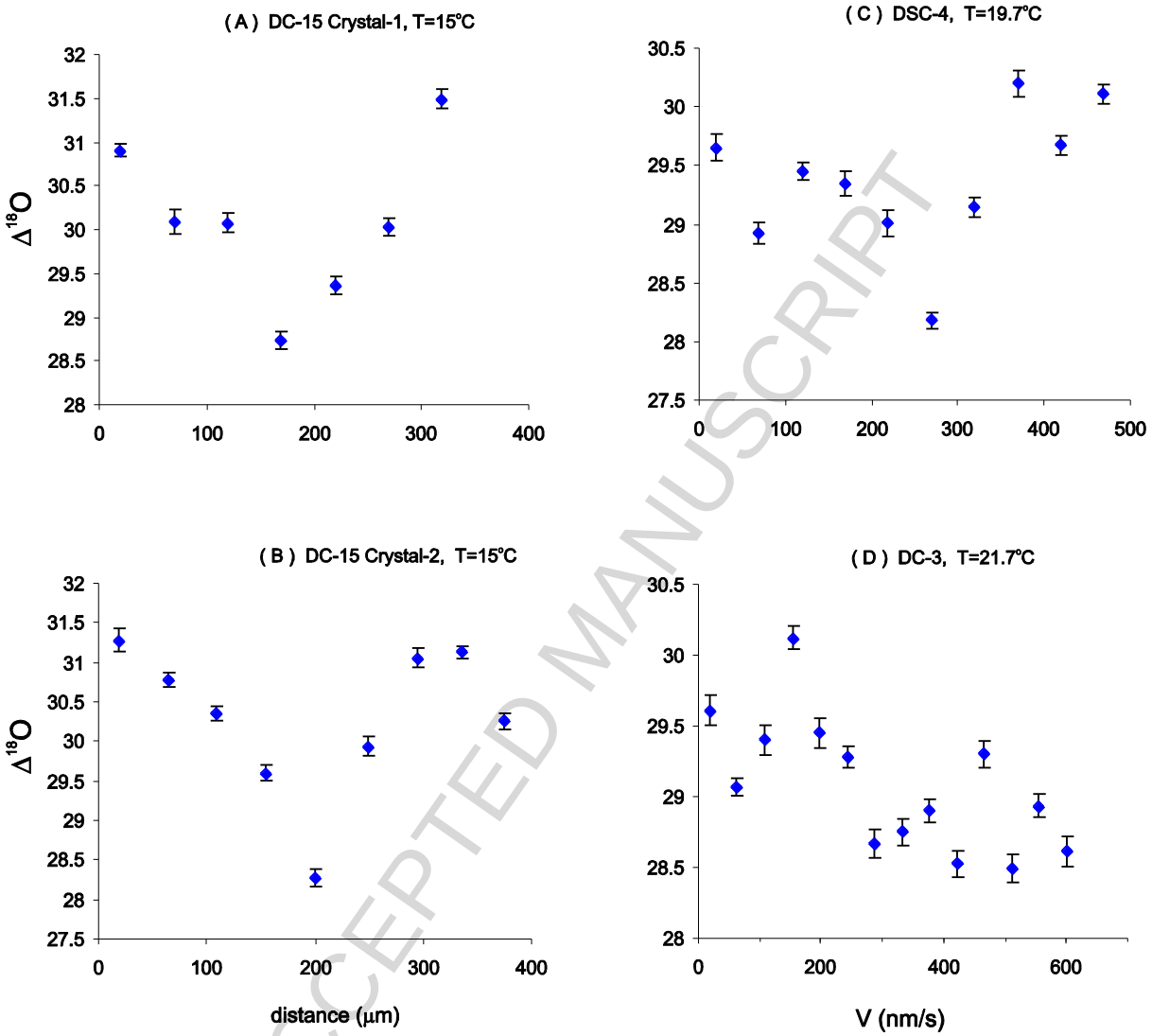

Figure 3

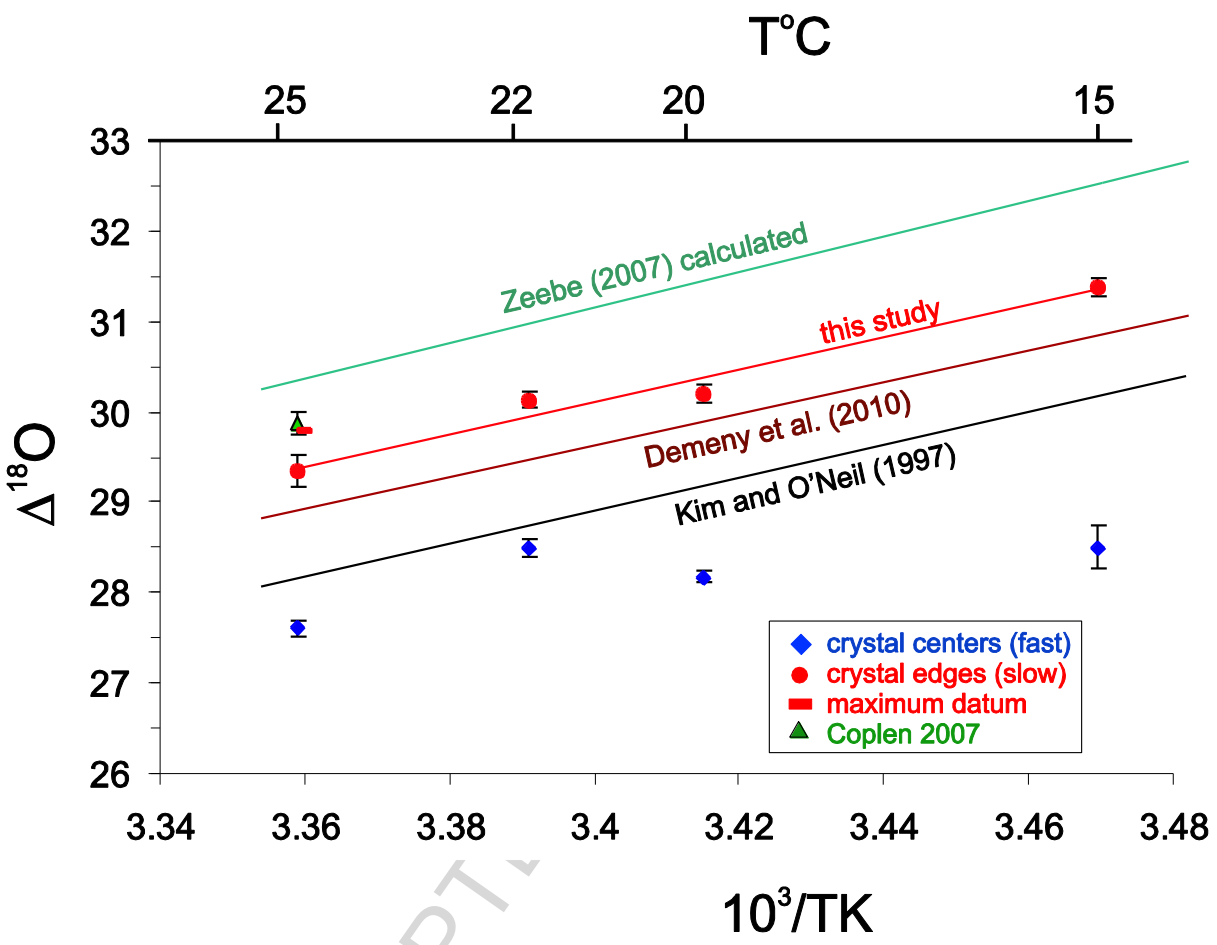

Figure 4

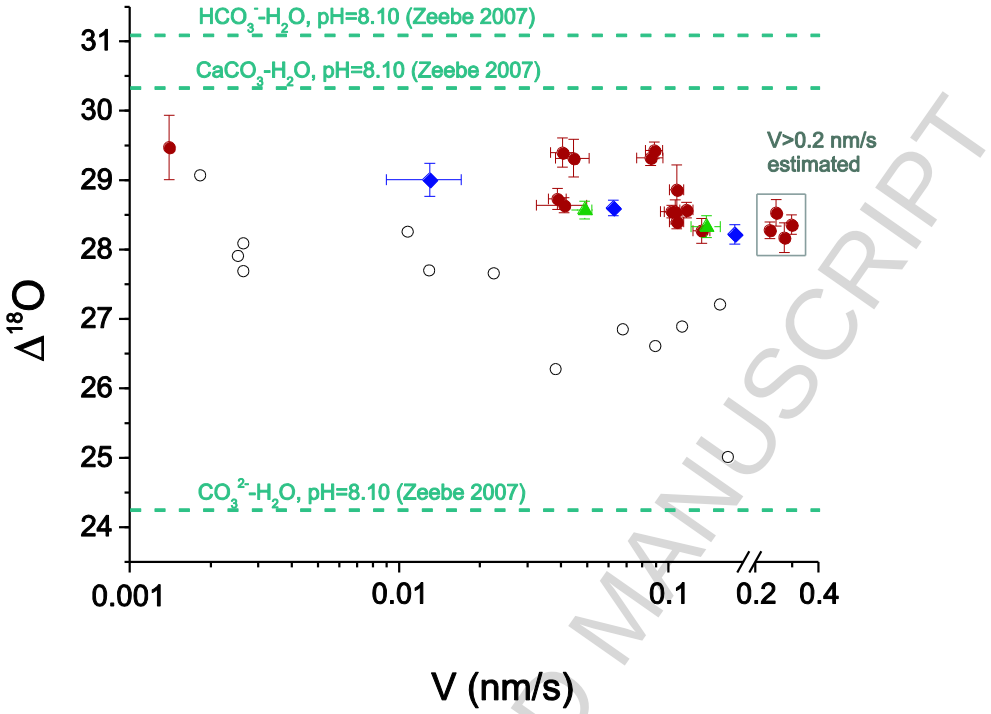

Figure 5

Highlights

> Calcite crystals were grown from aqueous solution under controlled conditions
> Intracrystal SIMS analyses revealed core-to-rim changes in $\alpha^{18}O_{calcite\text{-}fluid}$
> $\alpha^{18}O_{calcite\text{-}fluid}$ decreases with increasing growth rate toward $\alpha^{18}O_{eq(CO_3^{2-}\text{-}fluid)}$
> $\alpha^{18}O_{calcite\text{-}fluid}$ approaches equilibrium at the slowest growth rate
> $\alpha^{18}O_{calcite\text{-}fluid}$ as $f(T)$ is closer to the equilibrium relation than previous studies